Zhang et al. Nanoscale Research Letters (2016) 11:302
DOI 10.1186/s11671-016-1516-4

Nanoscale Research Letters

NANO REVIEW Open Access

# Preparation and Application of $TiO_2$ Nanotube Array Gas Sensor for $SF_6$-Insulated Equipment Detection: a Review

Xiaoxing Zhang[1,2*], Yingang Gui[1] and Xingchen Dong[1]

## Abstract

Since Zwilling and co-workers first introduced the electrochemical anodization method to prepare $TiO_2$ nanotubes in 1999, it has attracted a lot of researches due to its outstanding gas response and selectivity, making it widely used in gas detection field. This review presents an introduction to the sensor applications of $TiO_2$ nanotube arrays (TNTAs) in sulfur hexafluoride ($SF_6$)-insulated equipment, which is used to evaluate and diagnose the insulation status of $SF_6$-insulated equipment by detecting their typical decomposition products of $SF_6$: sulfur dioxide ($SO_2$), thionyl fluoride ($SOF_2$), and sulfuryl fluoride ($SO_2F_2$). The synthesis and sensing properties of $TiO_2$ nanotubes are discussed first. Then, it is followed by discussing the theoretical sensing to the typical $SF_6$ decomposition products, $SO_2$, $SOF_2$, and $SO_2F_2$, which analyzes the sensing mechanism at the molecular level. Finally, the gas response of pure and modified $TiO_2$ nanotubes sensor to $SO_2$, $SOF_2$, and $SO_2F_2$ is provided according to the change of resistance in experimental observation.

## Review

### Introduction

Titanium dioxide ($TiO_2$) nanotube has been widely researched due to its distinguished properties, including high surface-to-volume ratios, high surface activity, strong catalytic activity, and high ultraviolet light adsorption and heat conductivity [1–3]. It has been used in fields such as industrial manufacturing, aerospace, ocean exploring, environmental protection, resource development, and medical diagnose [4–7]. To meet the increasing high requirement for gas detection, $TiO_2$ nanotube gas sensors are investigated for qualitative or quantitative gas detection. However, the detection response, selectivity, and accuracy of pure $TiO_2$ are limited for different gases detection. To improve its detection performance, the most used methods are morphology control and surface modification [2, 8, 9], aiming to increase the effective reaction surface and active site. For common gas detection such as $O_2$, $H_2$, $SO_2$ and $H_2S$, the highest detection limit has even reaches parts per million level [10–14].

Sulfur hexafluoride ($SF_6$) insulating gas possesses outstanding arc quenching and insulation performance, which is the most used filled gas in gas-insulated equipment, such as gas-insulated switchgear (GIS), gas-insulated lines (GIL), and gas circuit breaker (GCB) [15–17]. However, $SF_6$ gas will inevitably decomposes to various typical decomposition components: $SO_2$, $SOF_2$, $SO_2F_2$, etc. under partial discharge and disruptive discharge (surface flashover and creeping discharge) when insulation defects occurs in production and long term operation process [18–20]. The insulation defects in $SF_6$-insulated equipment show great influence on the stability of entire insulated system. On the one hand, the dielectric strength of filled insulated gas obviously reduces under discharge because of the decomposition of $SF_6$. On the other hand, the decomposition components (low-fluorine sulfides) corrode the surface of $SF_6$-insulated equipment with the action of trace water and oxygen in equipment [21]. Besides, most of the insulation defect-induced discharge is hard to be found by the inspection workers as the discharge is always unsustainable. Therefore, online detection method, which assesses the insulation status automatically in real time, becomes an effective to solve the detection difficulty [22–24]. However, the current detections methods: ultra

* Correspondence: xiaoxing.zhang@outlook.com
[1]State Key Laboratory of Power Transmission Equipment and System Security and New Technology, Chongqing University, Chongqing 400044, China
[2]School of Electrical Engineering, Wuhan University, Wuhan 430072, China

high frequency (UHF) method, transient earth voltage (TEV) method, ultrasonic method, and fluorescence detection method are easily affected by the environmental interference signal [25–28]. Thanks to the distinguished anti-interference and high detection precision properties of gas sensors detection method, online gas detection becomes a new breakthrough for insulation status assessment of $SF_6$-insulted equipment.

In this paper, we will review the achievements in the filed using $TiO_2$ nanotubes for three typical $SF_6$ decomposition components: $SO_2$, $SOF_2$, and $SO_2F_2$ detection. Firstly, pure morphology of $TiO_2$ nanotubes is prepared by adopting different preparation methods. In addition, the surface modification of $TiO_2$ nanotubes is analyzed by experimental study to enhance the gas detection response. Secondly, the gas sensing properties are discussed to analyze the gas detection mechanism by theoretical studies. Finally, the gas sensing property to three typical $SF_6$ decomposition products is discussed by theoretical and experimental studies. Meanwhile, the influence factors such as gas concentration and sensing time are presented in detail.

## Synthesis of $TiO_2$ Nanotubes

Assisted-template method is one of the effective methods to synthesize $TiO_2$ nanotubes, as the synthesized $TiO_2$ nanotubes reported by Hyunjung et al. shown in Fig. 1a [29]. In terms of the preparation process, it is fabricated by filling the nano-structural unit into the hole of different templates, including anodic aluminum oxide (AAO) template, high polymer template, porous silica template and mesoporous zeolite, etc. AAO template is one of the most used method to synthesize of $TiO_2$ nanotubes [30]. Firstly, AAO is prepared by anodization method to serve as the template to produce the polymer mold. Then, amorphous $TiO_2$ is electrochemically deposited to the hole of the AAO template. After high-temperature anneal, the amorphous $TiO_2$ turns to $TiO_2$ nanotubes, which shares the same diameter with the hole of AAO template. Finally, the $TiO_2$ nanotubes are received

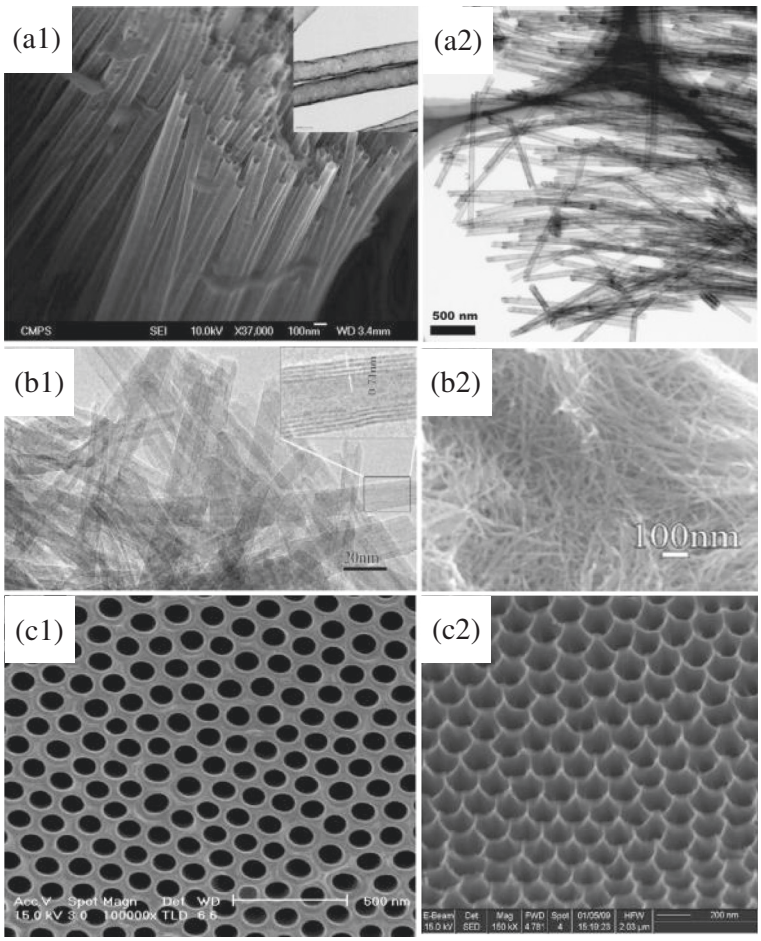


**Fig. 1** $TiO_2$ nanotubes synthesized by different methods: **a1**, **a2** Assisted-template method, **b1**, **b2** hydrothermal treatment method, and **c1**, **c2** anodization method

by dissolving the AAO template with strong alkali solution. Martine et al. successfully fabricated different kinds of metal nanotubes: $TiO_2$, $Co_3O_4$, $MnO_2$, $WO_3$, and ZnO nanotubes by this method [31]. In other study, Peng et al. fabricated bamboo-shaped $TiO_2$ nanotubes with an average diameter of 100 nm by upright dipping manner [32]. The bamboo-shaped nanotubes consist of many hollow compartments that are separated by $TiO_2$ layer.

Due to the features of simple and low-price preparation, hydrothermal treatment method is an effective method to synthesize $TiO_2$ nanotubes in large scale industrial production. The morphology of the produced $TiO_2$ nanotubes are usually composed by small diameter, thin wall, and large surface area nanotubes, and the nanotubes are usually unordered and intertwined as shown in Fig. 1b [33]. For the synthesis of $TiO_2$ nanotubes, firstly, mixing the $TiO_2$ nanoparticles with strong alkali solution under high temperature and high pressure, the single-layer nanosheets of $TiO_2$ appear in the treatment process curl from one dimension to two and three dimensions, which is similar with the formation mechanism of carbon nanotubes. After the chemical reactions, the $TiO_2$ nanotubes is received by ion-exchange and anneal. Finally, the powder-like $TiO_2$ nanotubes is obtained by centrifuged by centrifugal machine after neutralizing the strong alkali solution with weak acid solution. According to the report of Weng et al. in 2006 [34], $TiO_2$ nanotubes, with an external diameter of around 8 nm and a wall thickness of about 1 nm, was synthesized by hydrothermal treatment method.

The anodization method is one of the effective ways to synthesize ordered alignment and aspect radio $TiO_2$ nanotubes as shown in Fig. 1c [35]. The anodic Ti foil dissolve (metal corrosion or electropolishing) to Ti metal cation under the action of electrolyte and electric field. On the one hand, the produced Ti metal cation reacts with the $O^{2-}$ (produced by water electrolysis) and forms a $TiO_2$ oxidation film on the surface of Ti foil, resulting in the increase of resistance. Therefore, the formation rate of $TiO_2$ oxidation film decreases. On the other side, the produced $TiO_2$ oxidation film is dissolved by the electrolyte. Under the combined action of formation and dissolution, nanotube arrays synthesize on the surface of Ti foil. The nanotube morphology depends on many influence factors: applied voltage, electrolyte composition, and pH value. In 2000, Grimes et al. presented that an aligned and organized $TiO_2$ with an average tube diameter from 25 to 65 nm nanotubes fabricated by anodization method [36]. In addition, Grimes reviewed the fabrication, properties of highly ordered $TiO_2$ nanotube arrays made by anodic oxidation of titanium in fluoride-based electrolytes [37]. They found that the length of $TiO_2$ tends to be longer in the weak acid electrolytes, and the wall of $TiO_2$ nanotubes becomes smoother in organic electrolytes.

Due to the outstanding properties, high surface area, ordered alignment, and morphology adjustability of $TiO_2$ nanotubes, it shows great potential in gas detection. However, the pure $TiO_2$ nanotubes are hard to meet the high detection requirement because of its limitation in gas response, detection range, response time, and operational temperature. In this regard, great efforts have been made to extend the gas detection properties. Currently, a few modification methods: metal decoration, doping, semiconductor composites are introduced to improve the gas sensing properties [38, 39]. Comparing the different modification methods, metal decoration is one of the most effectively method to significantly enhance the gas response of $TiO_2$.

Metal decoration can be achieved in two different ways: metal nanoparticles decoration and metal ions decoration. For metal nanoparticles decoration, the metal nanoparticles are loaded or deposited on the surface of pure $TiO_2$ nanotubes to change the electron distribution in $TiO_2$ nanotubes system. For metal ions decoration, the ions are intruded into $TiO_2$ lattice, resulting in a trace of metal ions take the place of Ti atoms in the $TiO_2$ lattice by physical and chemical approaches. The decorated metal atoms improve the gas sensing properties by changing the electron distribution and energy band. Xiaoxing et al. synthesized Pt atom modified $TiO_2$ nanotubes in $H_2PtCl_6{\cdot}6H_2O$ (1 g/L) and $H_3BO_3$ (20 g/L) electrolytes by pulsed electrodeposition [40], which show good response to $SF_6$ decomposition products: $SO_2$, $SOF_2$, and $SO_2F_2$. Shahin el al. reported that the Au- and Ag-decorated $TiO_2$ nanotubes sensor exhibited a large resistance variation in the presence of very small quantities of $H_2$ gas at 25 °C [31].

## Theoretical Studies

In order to evaluate and diagnose the insulation status of $SF_6$-insulated equipment, it is necessary to precisely detect each kind of decomposition products of $SF_6$: $SO_2$, $SOF_2$, and $SO_2F_2$, respectively. However, these three kinds of gas products usually appear at the same time when discharge occurs in $SF_6$-insulated equipment, leading to

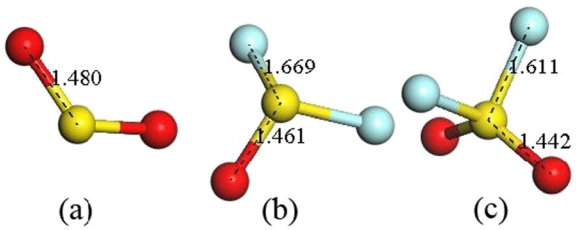


**Fig. 2** Structure of the gas molecules: **a** $SO_2$ molecule, **b** $SOF_2$ molecule, and **c** $SO_2F_2$ molecule. S, O, and F atoms are respectively shown in *red*, *yellow*, and *cyan*

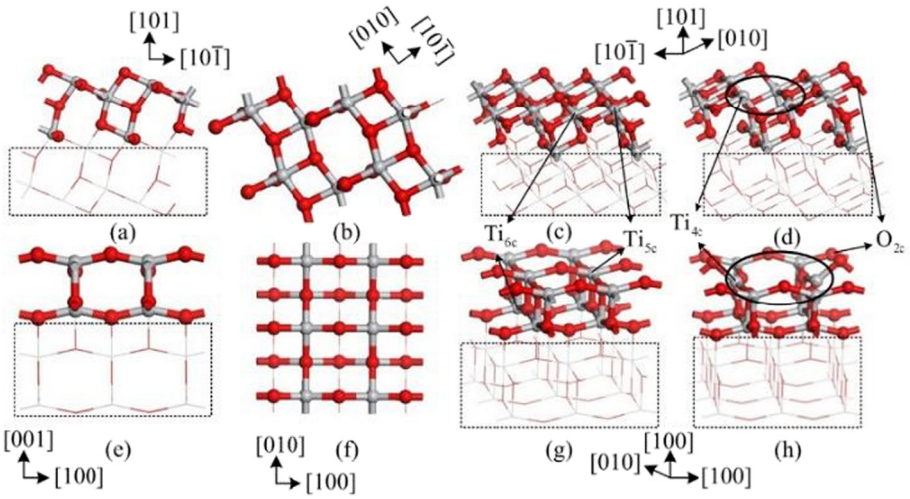


**Fig. 3** Four kinds of surfaces. **a**–**c** The views of (1 0 1) perfect surface. **d** (1 0 1) defect surface. **e**–**g** The views of (0 0 1) perfect surface. **h** (0 0 1) defect surface. Ti and O atoms are shown in *gray* and *red*, respectively. $Ti_{6c}$, $Ti_{5c}$, and $O_{2c}$ are marked by *arrows*, and oxygen vacancy sites are marked by *ellipse*

the cross interference between different products. Therefore, a lot of researches have been made to enhance the gas selectivity while improving the gas response.

This section mainly discusses the theoretical studies employed to analyze the sensing mechanism to $SO_2$, $SOF_2$, and $SO_2F_2$. Xiaoxing's group has conducted a lot of researches in online monitoring for $SF_6$-insulated equipment by theoretical simulation method based on DMol$^3$ module of materials studio [20, 22, 23, 41, 42]. It provides an effective way to explain the sensing mechanism at the molecular level by analyzing the adsorption energy, states of density, and energy band structure. Before gas molecules adsorption on the surface of $TiO_2$, the structure of $SO_2$, $SOF_2$, $SO_2F_2$, and pure $TiO_2$ are respectively optimized as shown in Figs. 2 and 3 [42]. As can be seen in Fig. 3, four surfaces, (1 0 1) perfect surface, (1 0 1) defect surface, (0 0 1) perfect surface, and (0 0 1) defect surface, are presented to analyze the different

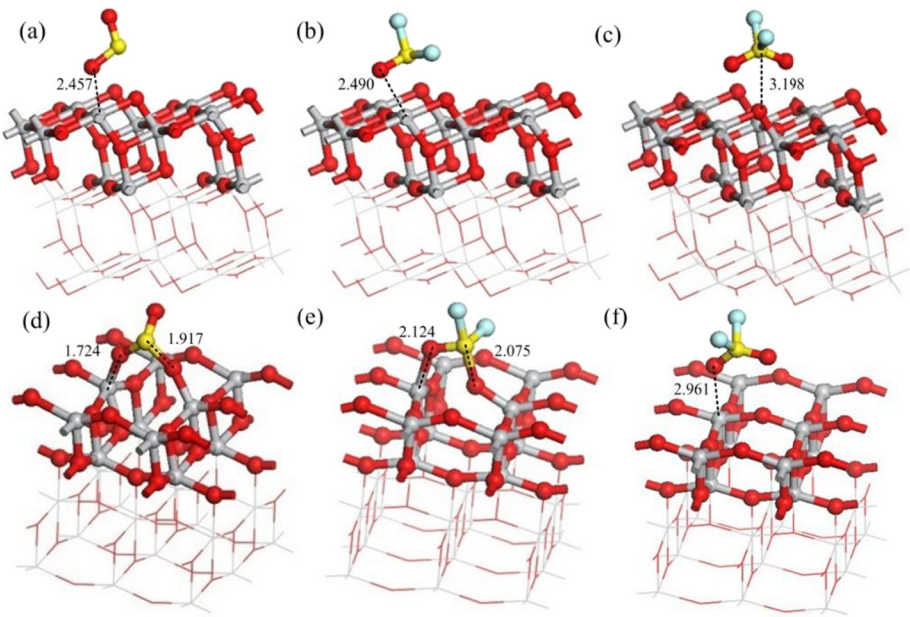


**Fig. 4** Adsorption structures of gas molecules on perfect surfaces: **a** $SO_2$ adsorbs on the (1 0 1) perfect surface, **b** $SOF_2$ adsorbs on the (1 0 1) perfect surface, **c** $SO_2F_2$ adsorbs on (1 0 1) perfect surface, **d** $SO_2$ adsorbs on the (0 0 1) perfect surface, **e** $SOF_2$ adsorbs on the (0 0 1) perfect surface, and **f** $SO_2F_2$ adsorbs on the (0 0 1) perfect surface. Binding distances are in Å

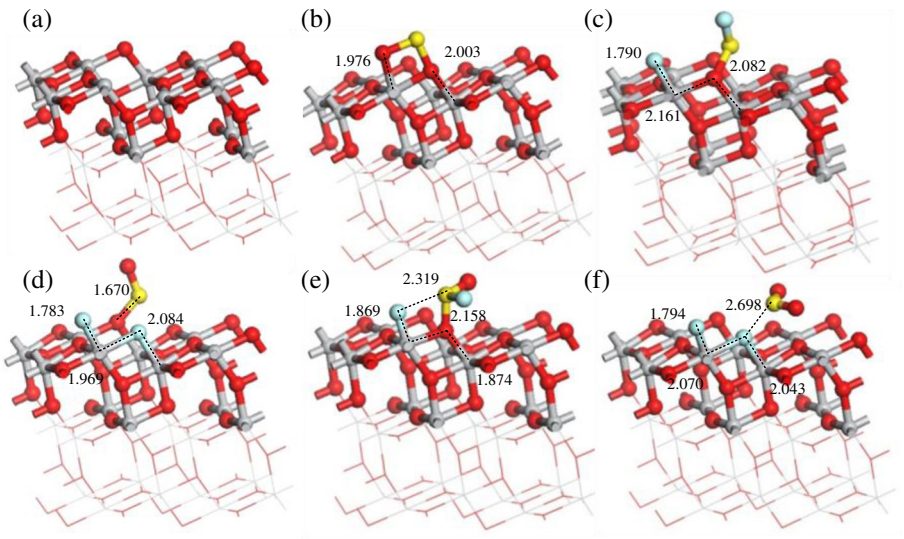


**Fig. 5** Adsorption structures of the gas molecules on the (1 0 1) defect surface: **a** The clear (1 0 1) defect surface, **b** $SO_2$ adsorption, **c**, **d** $SOF_2$ adsorption with different initial positions, and **e**, **f** $SO_2F_2$ adsorption with different initial positions. Binding distances are in Å

adsorption in detail. The PBE function is taken as the generalized gradient approximation to deal with the exchange-correlation energy in the whole simulation. To ensure the computation accuracy, the density functional computation adopts the double numerical basis set including p-polarization function. And the energy convergence, electronic self-consistent field, maximum force and displacement are respectively set as $1 \times 10^{-5}$ Ha, $1 \times 10^{-6}$ Ha, $2 \times 10^{-3}$ Ha/Å, and $5 \times 10^{-3}$ Å. The brillouin zone is sampled by $3 \times 1 \times 2$ and $3 \times 3 \times 1$ for (1 0 1) and (0 0 1) surface models, respectively [42]. According to the computation results of energy band, the computational value of energy gap (2.161 eV) is consistent with other computational results, though it is smaller than its experimental value (3.23 eV) (Fig. 4).

### *(1 0 1) and (0 0 1) Perfect Surface of $TiO_2$*

Figure 5 shows the adsorption structures of $SO_2$, $SOF_2$, and $SO_2F_2$ on the (1 0 1) and (0 0 1) perfect surface of $TiO_2$ nanotubes [42]. The adsorption energy, charge transfer, binding distance, and energy gap are shown in Table 1. The adsorption energy and charge transfer decrease in the following order: $SO_2 > SOF_2 > SO_2F_2$ on both of the surfaces, respectively. But both of the adsorption energy and charge transfer on (0 0 1) surface are distinctly larger than that on (1 0 1) surface for all gas molecules, indicating that gas molecules are physisorbed on (1 0 1) surface and chemisorbed on (0 0 1) surface. Comparing the sensing properties to these three gas molecules, the (1 0 1) and (0 0 1) perfect surface of $TiO_2$ show better adsorption property to $SO_2$ than $SOF_2$ and $SO_2F_2$.

### *Oxygen-Defect (1 0 1) Surface of $TiO_2$*

As shown in Fig. 3, different adsorption sites are discussed for $SO_2$, $SOF_2$, and $SO_2F_2$ adsorption on oxygen vacancy induced (1 0 1) defect surface of $TiO_2$ [42]. The energy gap of (1 0 1) defect surface (1.888 eV) is distinctly smaller than that of (1 0 1) perfect surface (1.951 eV). For $SO_2$ adsorption, one sulfur atom takes the place of oxygen vacancy and the other sulfur atom interacts with Ti atoms. When $SOF_2$ adsorbs on (1 0 1) defect surface of $TiO_2$, the F-S bond of $SOF_2$ tends to break because of the strong chemisorption. Similarly, the F–S bond of $SO_2F_2$ breaks in the adsorption process seen in Fig. 3e, f. As a result, the conductivity of (1 0 1) defect surface increases after $SO_2$ and $SOF_2$ adsorption. Conversely, adsorption of $SO_2F_2$ increases the band gaps

**Table 1** Calculated adsorption energy, charge transfer, and binding distance of the perfect surfaces

| Surface | (1 0 1) perfect surface | | | | (0 0 1) perfect surface | | | |
|---|---|---|---|---|---|---|---|---|
| Structure | $TiO_2$ (1 0 1) | $SO_2$ | $SOF_2$ | $SO_2F_2$ | $TiO_2$ (0 0 1) | $SO_2$ | $SOF_2$ | $SO_2F_2$ |
| $E_a$ (eV) | \ | −0.360 | −0.297 | −0.214 | \ | −1.660 | −1.170 | −0.690 |
| Q (e) | \ | 0.097 | 0.051 | 0.010 | \ | −0.356 | −0.118 | 0.014 |
| d (Å) | \ | 2.457 | 2.490 | 3.198 | \ | 1.724 | 2.075 | 2.961 |
| $E_g$ (eV) | 1.951 | 1.788 | 1.932 | 1.936 | 1.613 | 1.488 | 1.565 | 1.602 |

**Table 2** Calculated adsorption energy, charge transfer, and binding distance of (1 0 1) defect surface

| Surface | (1 0 1) defect surface | | | | | |
|---|---|---|---|---|---|---|
| Structure | $TiO_2$ (1 0 1) | $SO_2$ (b) | $SOF_2$ (c) | $SOF_2$ (d) | $SO_2F_2$ (e) | $SO_2F_2$ (f) |
| $E_a$ (eV) | \ | −2.150 | −2.095 | −3.037 | −4.356 | −4.686 |
| Q (e) | \ | −0.699 | −0.183 | −0.734 | −0.978 | −0.877 |
| d (Å) | \ | 1.976 | 1.790 | 1.670 | 1.869 | 1.794 |
| $E_g$ (eV) | 1.888 | 1.524 | 1.250 | 1.283 | 1.932 | 1.935 |

**Table 3** Calculated adsorption energy, charge transfer, and binding distance of the (0 0 1) defect surface

| Surface | (0 0 1) defect surface | | | | | |
|---|---|---|---|---|---|---|
| Structure | $TiO_2$ (0 0 1) | $SO_2$ (b) | $SOF_2$ (c) | $SOF_2$ (d) | $SO_2F_2$ (e) | $SO_2F_2$ (f) |
| $E_a$ (eV) | \ | −3.205 | −3.095 | −4.810 | −4.807 | −4.786 |
| Q (e) | \ | −0.603 | −0.701 | −0.996 | −0.978 | −0.929 |
| d (Å) | \ | 1.925 | 1.830 | 1.777 | 1.886 | 1.776 |
| $E_g$ (eV) | 1.385 | 1.263 | 1.469 | 1.204 | 1.562 | 1.499 |

and reduces the conductivity of the (1 0 1) defect surface (Table 2).

### *Oxygen-Defect (0 0 1) Surface of $TiO_2$*

Figure 6 presents the adsorption structures of $SO_2$, $SOF_2$, and $SO_2F_2$ on the oxygen-defect (0 0 1) surface of $TiO_2$ [42]. The sulfur atoms of $SO_2$ molecule interact with the Ti atoms with bonding distance of 1.853 Å by physisorption as shown in Fig. 6b. When $SOF_2$ and $SO_2F_2$ molecule adsorb on the surface with different initial positions as shown in Fig. 6c, d, the structures break because of the strong chemisorption. As the adsorption energy and charge shown in Table 3, the (0 0 1) defect surface of $TiO_2$ shows stronger adsorption than (1 0 1) defect surface. The $SO_2$ and $SOF_2$ adsorption increase the conductivity of (0 0 1) defect surface by introducing the impurity state between valence and conduction band. While $SOF_2$ adsorption leads to the decrease of conductivity of the (0 0 1) defect surface according to the widened energy gap.

### *Pt-Decorated (1 0 1) Surface of $TiO_2$*

Pt atoms decoration $TiO_2$ is widely used to enhance the gas response in different gas detection field. In this section, we present the theoretical computation of Pt-decorated (1 0 1) surface of $TiO_2$ and its gas response to $SO_2$, $SOF_2$, and $SO_2F_2$. As the structure of pure and Pt-decorated (1 0 1) surfaces of $TiO_2$ shown in Fig. 7, the Pt atom builds a stable structure with two oxygen atoms. Figure 8 shows the density of states (DOS) of (1 0 1) perfect surface and Pt-decorated (1 0 1) surface of $TiO_2$. It is found that the separated valence and conductive bond become continuous after Pt decoration, signifying the increasing conductivity of $TiO_2$ (1 0 1) surfaces.

Considering that Pt decoration on the surface of $TiO_2$ (1 0 1) is usually in the form of Pt particles, three

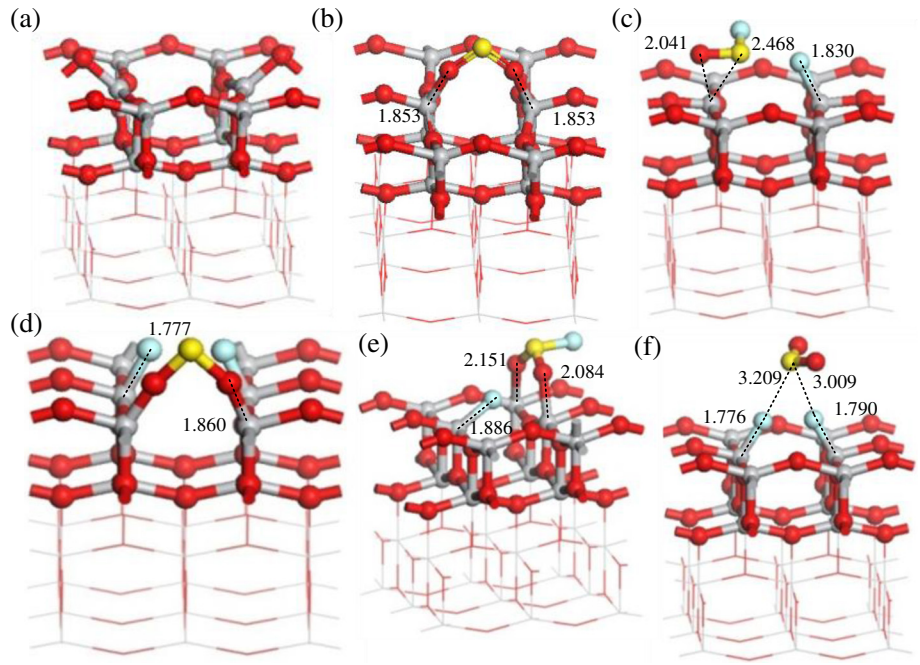


**Fig. 6** Adsorption structures of the gas molecules on the (0 0 1) defect surface: **a** The clear (0 0 1) defect surface, **b** $SO_2$ adsorption, **c**, **d** $SOF_2$ adsorption with different initial positions, and **e**, **f** $SO_2F_2$ adsorption with different initial positions. Binding distances are in Å

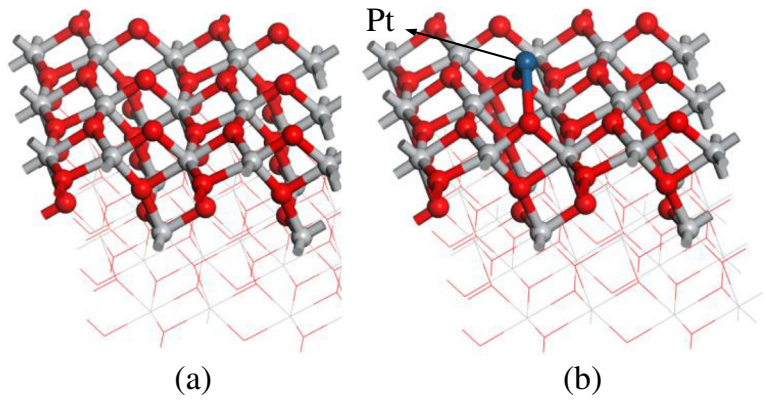


**Fig. 7 a** (1 0 1) perfect surface of $TiO_2$; **b** Pt-decorated (1 0 1) surface of $TiO_2$

different adsorption situations for $SO_2$, $SOF_2$, and $SO_2F_2$ are discussed in Fig. 9. Figure 9a1–a3 show the adsorption of $SO_2$, $SOF_2$, and $SO_2F_2$ on the surface of $TiO_2$ (1 0 1) perfect surface away from Pt atom. The Pt decoration brings little influence to the adsorption of $SO_2$, $SOF_2$, and $SO_2F_2$ molecules; three molecules are physisorbed on the $TiO_2$ (1 0 1) perfect surface, indicating that the enhancement of gas sensing comes from the adsorption around Pt atoms. Figure 9b1–b3 present the adsorption of $SO_2$, $SOF_2$, and $SO_2F_2$ at the boundary between Pt atom and $TiO_2$ (1 0 1) perfect surface. The Pt aom acts as the active site to adsorb the $SO_2$, $SOF_2$, and $SO_2F_2$ molecules. $SO_2$ and $SOF_2$ prefer to approach the Pt atom by sulfur atom with nearest binding distances of 2.363 and 2.263 Å, respectively, while $SO_2F_2$ approaches to the Pt atom by oxygen atom of $SO_2F_2$. For $SO_2$, $SOF_2$, and $SO_2F_2$ adsorption on the surface of Pt particles, a (2 0 0) surface of Pt metal is considered in the study as shown in Fig. 9c1–c3; the $SO_2$ and $SOF_2$ molecules interact with Pt atom with distances of 2.299 and 2.312 Å. And the interaction between (2 0 0) surface of Pt metal and $SO_2F_2$ promotes the decomposition of $SO_2F_2$.

## Experimental Observations

### *Pure $TiO_2$*

In this section, the gas response (change of resistance) of $TiO_2$ nanotube arrays (TNTAs) to $SO_2$, $SOF_2$ and $SO_2F_2$ are discussed at 200 °C, and the negative value of resistance variation (R%) means the reduction of resistance. According to the correspondence between gas response and concentration, it is found that the change between them presents a fitting curve relationship. As a result, we can directly estimate the concentration of gas according to the corresponding gas response.

Figure 10a1, a2 show the gas response to $SO_2$ with different concentration: 10, 20, 30, 40, and 50 ppm [40]; the horizontal and vertical ordinate present the gas sensing time and gas response, respectively. It is found that the resistance of TNTAs rapidly decreases when it contacts with $SO_2$ and eventually reaches a stable value with time. The $SO_2$ response to 10, 20, 30, 40, and 50 ppm are −14.35, −25.23, −40.16, −57, and −74.6 %, respectively. And a fitting line: $y = -1.523x + 3.409$ with fit goodness of 0.992 is obtained. According to the change of resistance shown in Fig. 10b1, b2, the resistance decrease after $SOF_2$ detected by TNTAs at 200 °C. In addition, the gas sensing time increase with the

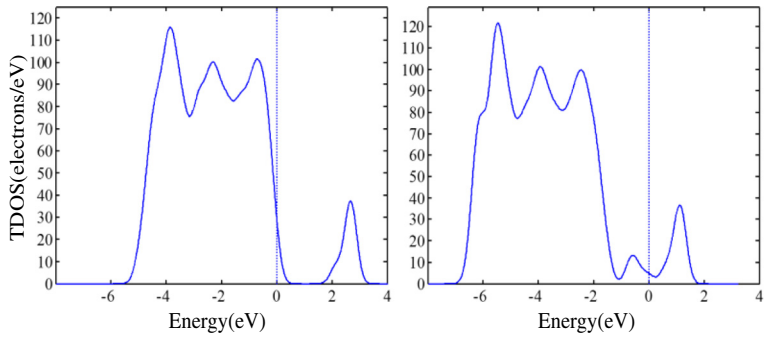


**Fig. 8 a** DOS of $TiO_2$ (1 0 1) perfect surface; **b** DOS of $TiO_2$ Pt-decorated (1 0 1) surface

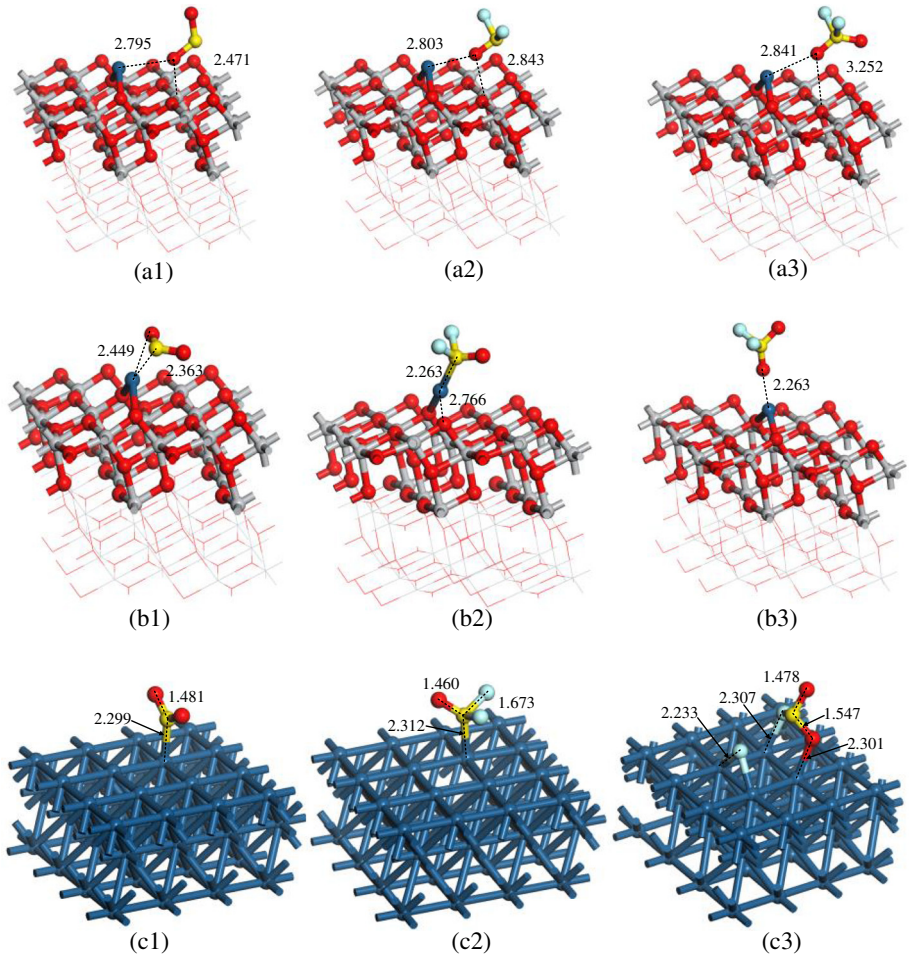


**Fig. 9** Adsorption structures of the gas molecules on different sites of Pt-decorated (1 0 1) surface (**a1**)-(**a3**) adsorption of $SO_2$, $SOF_2$ and $SO_2F_2$ on Pt doped $TiO_2$ (1 0 1) perfect surface away from Pt atom, (**b1**)-(**b3**) adsorption of $SO_2$, $SOF_2$ and $SO_2F_2$ at the boundary between Pt atom and $TiO_2$ (1 0 1) perfect surface, (**c1**)-(**c3**) adsorption of $SO_2$, $SOF_2$ and $SO_2F_2$ on Pt atoms

concentration with $SO_2$. The response to 30, 50, 70, and 100 ppm $SOF_2$ are −2.38, −7.82, −15.95, and −22.13 %, respectively. And the fitting line is $y = -0.289x + 6.023$ with fit goodness of 0.982. Although the resistance of $TiO_2$ nanotubes array decreases during $SO_2F_2$ contacting, the change of resistance is obviously smaller than that of $SO_2$ and $SOF_2$ sensing at the same gas concentration and temperature. The highest gas response is only −8.37 % when the concentration of $SO_2F_2$ reaches 100 ppm. The fitting line is $y = -0.062x - 2.368$ with fit goodness of 0.988.

Comparing the gas sensing speed and magnitude of resistance change at the same gas concentration and temperature, the gas response of TNTAs to $SF_6$ decomposition products is in orders, $SO_2 > SOF_2 > SO_2F_2$, indicating the potential of selective detection between $SO_2$, $SOF_2$, and $SO_2F_2$.

### *Pt-Decorated TNTAs*

Figure 11 presents the gas sensing property of Pt-decorated TNTAs (Pt-TNTAs) to $SO_2$, $SOF_2$, and $SO_2F_2$ at 150 °C [40, 43]. Due to the decoration of Pt particles on the surface of $TiO_2$ nanotubes, it not only enhances the gas response to $SOF_2$ and $SO_2F_2$ also reduces the working temperature for gas detection. As shown in Fig. 11a1–a2, the gas response to different concentrations of $SO_2$, 30, 50, 70, and 100 ppm are −5.31, −8.38, −15.18, and −24.07 %. After linear fitting, the corresponding relation between $SO_2$ concentration and gas response is $y = -0.276x + 4.405$ with fit goodness of 0.984. The change of resistance of Pt-TNTAs is obviously smaller than that of pure TNTAs in the $SO_2$ detection process. For instance, the gas response of pure TNTAs and Pt-TNTAS is −74.6 and −8.38 % when the concentration of $SO_2$ is 50 ppm. As shown in Fig. 11b1–b2, the response of Pt-TNTAs to 30, 50, 70, and 100 ppm $SOF_2$ are 3.23, −6.11, −12.92, and −23.75 %, respectively. And the fitting line is $y = -0.301x + 7.333$, indicating that the change of response to different concentration of $SOF_2$ is still linear. The response to $SOF_2$ slightly increases comparing with that of pure TNTAs at

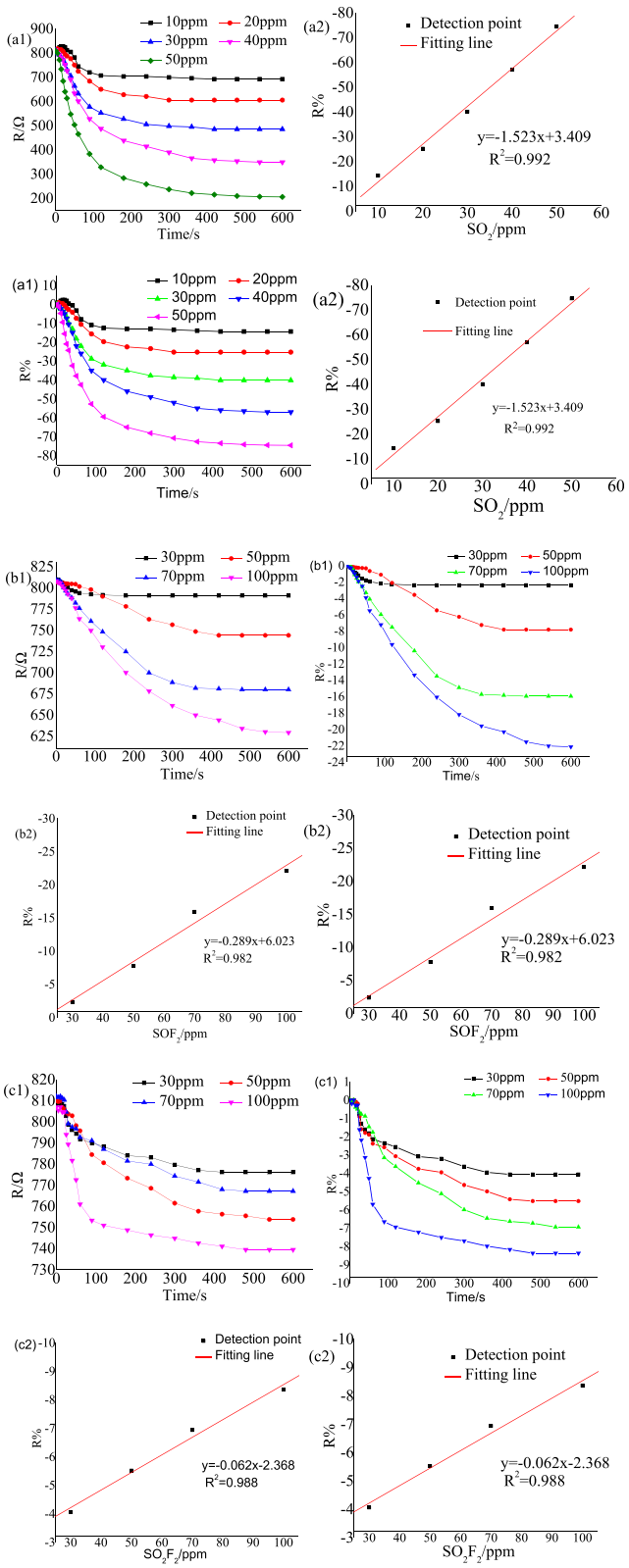


**Fig. 10** Pure TNTAs response to different $SF_6$ decomposition products at 200 °C. **a1**, **a2** SO2 sensing, **b1**, **b2** $SOF_2$ sensing, and **c1**, **c2** $SO_2F_2$ sensing

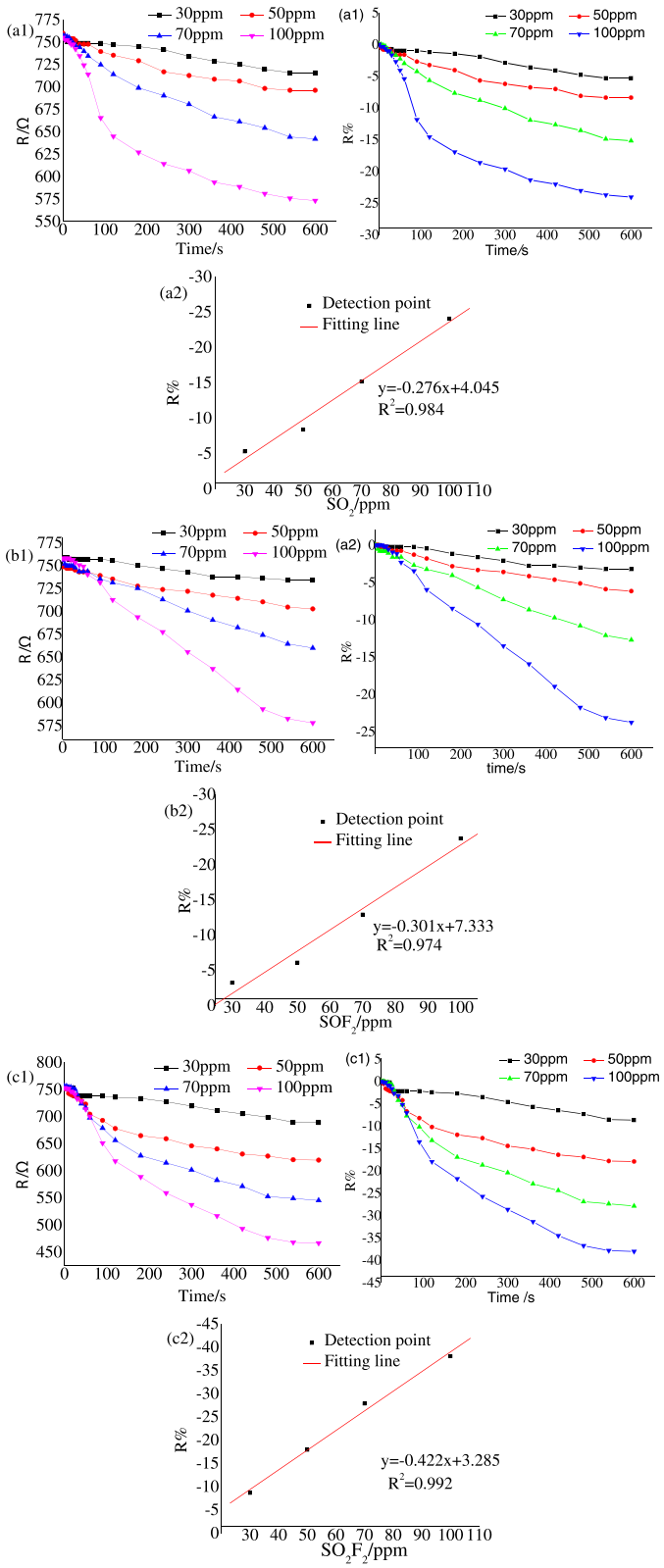


**Fig. 11** Pt-TNTAs response to different $SF_6$ decomposition products at 150 °C. **a1**, **a2** $SO_2$ sensing, **b1**, **b2** $SOF_2$ sensing, and **c1**, **c2** $SO_2F_2$ sensing

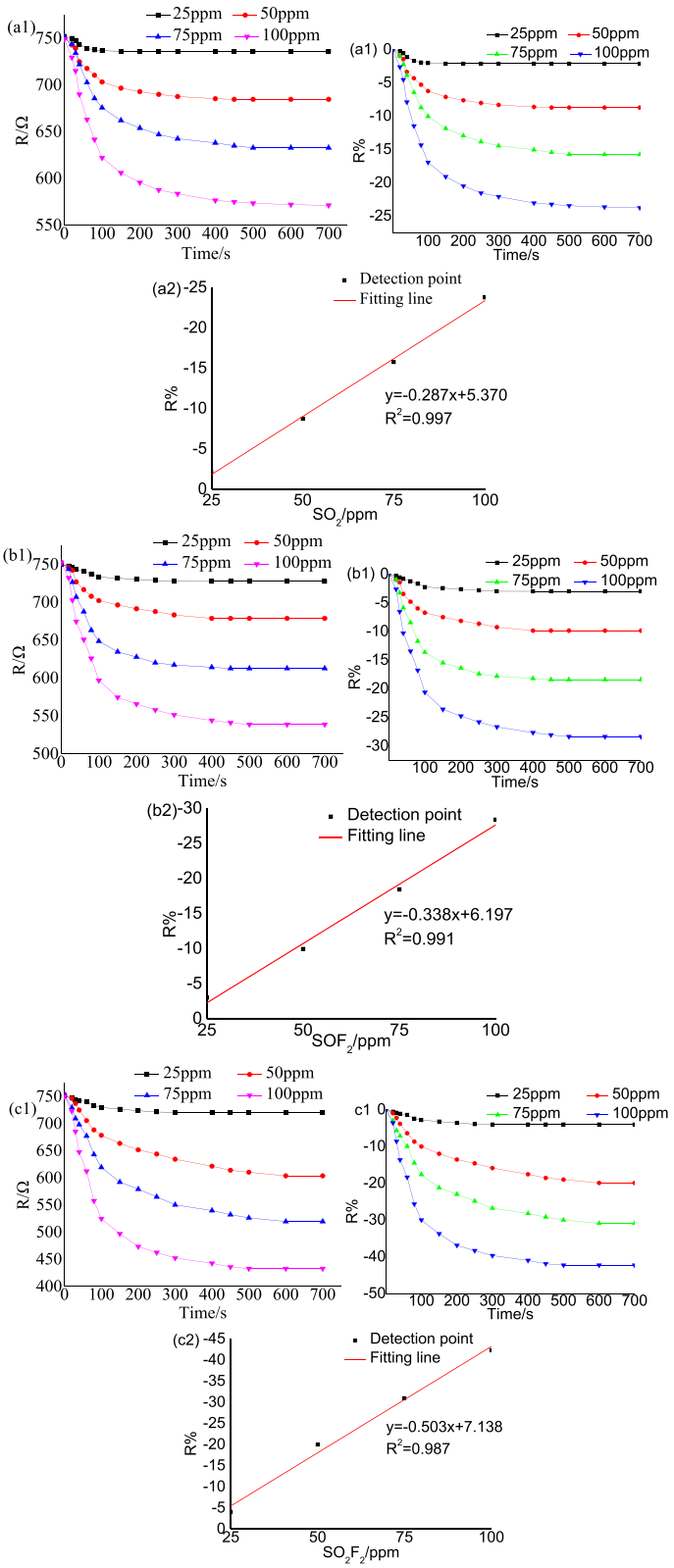


**Fig. 12** Au-TNTAs response to different $SF_6$ decomposition products at 110 °C. **a1**, **a2** $SO_2$ sensing, **b1**, **b2** $SOF_2$ sensing, and **c1**, **c2** $SO_2F_2$ sensing

the same $SOF_2$ concentration. Therefore, the improvement for $SOF_2$ detection from Pt decoration mainly reflects on the aspect of the working temperature reduction. As the gas response of Pt-TNTAs to $SO_2F_2$ shown in Fig. 11c1–c2, the change of resistance for 30, 50, 70, and 100 ppm of $SO_2F_2$ are −8.65, −17.91, −27.86, and −38.02 %. And a liner function ($y = -0.422x + 3.285$) is received with high fit goodness of 0.992. Comparing the gas response before and after Pt decoration, it is found that the gas response distinctly increases at the same $SO_2F_2$ concentration, indicating that the Pt-TNTAs possesses selective detection for $SO_2F_2$ after Pt particles decoration.

### *Au-Decorated TNTAs*

The gas response of Au-decorated TNTAs (Au-TNTAs) to $SO_2$, $SOF_2$ and $SO_2F_2$ are discussed in this section as shown in Fig. 12. The working temperature (120 °C) applied in the detection process is much lower than that of pure TNTAs and Pt-TNTAs sensors, which is benefit for wide spread application. Fitting the resistance with different concentration of $SO_2$, $SOF_2$, and $SO_2F_2$ (25, 50, 75, and 100 ppm) shown in Fig. 12a2–c2, the response of Au-TNTAs to different kinds of $SF_6$ decomposition components is in the following order: $SO_2F_2 > SOF_2 > SO_2$. Comparing the gas response property of pure TNTAs, Pt-TNTAs and Au-TNTAs sensors to $SF_6$ decomposition components, metal decoration not only enhances the gas response to the decomposition components but also realizes the selective detection to different decomposition components. In addition, metal decoration effectively reduces the working temperature.

## Conclusions

$TiO_2$ nanotube arrays (TNTAs) has been widely used as gas sensor for its distinguished properties in large specific surface area, large pore structure, easy synthesis process, and environmentally friendly nature. In order to evaluate and diagnose the insulation status of $SF_6$-insulated equipment, TNTAs gas sensor becomes an effective new method to realize the function by detecting the decomposition components of $SF_6$: $SO_2$, $SOF_2$, and $SO_2F_2$. In terms of TNTAs synthesis, three methods, assisted-template method, hydrothermal treatment method, and anodization method, are discussed to analyze the preparation process and the features of prepared TNTAs in detail. Then, recent studies carried out by theoretical simulation have been viewed. The adsorption of $SO_2$, $SOF_2$, and $SO_2F_2$ on different surface of $TiO_2$ is reviewed in this section, including (1 0 1) and (0 0 1) perfect surface of $TiO_2$, oxygen-defect (1 0 1) and (0 0 1) surface of $TiO_2$, and Pt-decorated (1 0 1) surface of $TiO_2$. Finally, the experimental researches used to analyze the gas response of TNTAs sensor to $SO_2$ and $SOF_2$ and $SO_2F_2$ are discussed. Comparing the gas response to $SO_2$, $SOF_2$, and $SO_2F_2$ by different gas sensors (pure TNTAs sensor and Pt, Au-decorated TNTAs sensor), it is found that the metal decoration improves the gas response property to $SO_2$ and $SOF_2$ and $SO_2F_2$ and also reduces the working temperature for gas detection. Further, more studies should be investigated to enhance the detection precision and stability of TNTAs, aiming to industrialize the fabrication and application of TNTAs sensor in $SF_6$-insulated equipment.

#### Competing interests

The authors declare that they have no competing interests.

#### Authors' contributions

The paper was written by YGG. The experimental section was provided by XXZ. All revisions were discussed by XXZ, YGG, and XCD. All authors read and approved the final manuscript.

#### Acknowledgements

This work was supported by the National Natural Science Foundation of China under Project no. 51277188.

Received: 13 April 2016 Accepted: 2 June 2016
Published online: 18 June 2016

#### References

1. Chen X, Mao SS (2007) Titanium dioxide nanomaterials: synthesis, properties, modifications, and applications. Chem Rev 107:2891–2959
2. Yang L, Luo S, Cai Q, Yao S (2010) A review on $TiO_2$ nanotube arrays: fabrication, properties, and sensing applications. Chin Sci Bull 55:331–338
3. Zheng Q, Zhou B, Bai J, Li L, Jin Z, Zhang J, Li J, Liu Y, Cai W, Zhu X (2008) Self-organized $TiO_2$ nanotube array sensor for the determination of chemical oxygen demand. Adv Mater 20:1044–1049
4. Zhang Q, Xu H, Yan W (2012) Highly ordered $TiO_2$ nanotube arrays: recent advances in fabrication and environmental applications—a review. Nanosci Nanotechnol Lett 4:505–519
5. Kalbacova M, Macak J, Schmidt-Stein F, Mierke C, Schmuki P (2008) $TiO_2$ nanotubes: photocatalyst for cancer cell killing. Physica Status Solidi (RRL)-Rapid Res Letters 2:194–196
6. Shankar K, Mor GK, Prakasam HE, Yoriya S, Paulose M, Varghese OK, Grimes CA (2007) Highly-ordered $TiO_2$ nanotube arrays up to 220 μm in length: use in water photoelectrolysis and dye-sensitized solar cells. Nanotechnology 18:065707
7. Xiong H, Slater MD, Balasubramanian M, Johnson CS, Rajh T (2011) Amorphous $TiO_2$ nanotube anode for rechargeable sodium ion batteries. J Phys Chem Lett 2:2560–2565
8. Cheng X, Xu Y, Gao S, Zhao H, Huo L (2011) Ag nanoparticles modified $TiO_2$ spherical heterostructures with enhanced gas-sensing performance. Sensors Actuators B: Chem 155:716–721
9. Wang C, Yin L, Zhang L, Gao R (2010) Ti/$TiO_2$ nanotube array/Ni composite electrodes for nonenzymatic amperometric glucose sensing. J Phys Chem C 114:4408–4413
10. Lu HF, Li F, Liu G, Chen ZG, Wang DW, Fang HT, Lu GQ, Jiang ZH, Cheng HM (2008) Amorphous $TiO_2$ nanotube arrays for low-temperature oxygen sensors. Nanotechnology 19:405504
11. Şennik E, Colak Z, Kılınç N, Öztürk ZZ (2010) Synthesis of highly-ordered TiO 2 nanotubes for a hydrogen sensor. Int J Hydrogen Energy 35:4420–4427
12. Morris D, Egdell R (2001) Application of V-doped $TiO_2$ as a sensor for detection of $SO_2$. J Mater Chem 11:3207–3210
13. Nisar J, Topalian Z, De Sarkar A, Österlund L, Ahuja R (2013) $TiO_2$-based gas sensor: a possible application to SO2. ACS Appl Mater Interfaces 5:8516–8522
14. Huang WF, Chen HT (2009) MLin. Density functional theory study of the adsorption and reaction of $H_2S$ on $TiO_2$ rutile (110) and anatase (101) surfaces. J Phys Chem C 113:20411–20420
15. T Ju, X Zhongrong, Z Xiaoxing, S Caixin (2007) GIS partial discharge quantitative measurements using UHF microstrip antenna sensors, in: Electrical Insulation and Dielectric Phenomena, 2007. CEIDP 2007. Annual Report-Conference on, IEEE. http://ieeexplore.ieee.org/xpls/abs_all.jsp?arnumber=4451454. pp. 116–119

16. O Völcker, H Koch (2000) Insulation co-ordination for gas-insulated transmission lines (GIL), in: Power Engineering Society Winter Meeting, 2000. IEEE, IEEE. http://ieeexplore.ieee.org/xpls/abs_all.jsp?arnumber=850143. pp. 703–711
17. J Liu, GM Huang, Z Ma (2010) A novel intelligent high voltage SF 6 circuit breaker, in: Power and Energy Society General Meeting, 2010 IEEE, IEEE. http://ieeexplore.ieee.org/xpls/abs_all.jsp?arnumber=5589436. pp. 1–6
18. Tang J, Zeng F, Pan J, Zhang X, Yao Q, He J, Hou X (2013) Correlation analysis between formation process of SF 6 decomposed components and partial discharge qualities. Dielectrics Electrical Insulation IEEE Trans 20:864–875
19. Zeng F, Tang J, Fan Q, Pan J, Zhang X, Yao Q, He J (2014) Decomposition characteristics of $SF_6$ under thermal fault for temperatures below 400 °C. Dielectrics Electrical Insulation IEEE Trans 21:995–1004
20. Zhang X, Gui Y, Dai Z (2014) A simulation of Pd-doped SWCNTs used to detect $SF_6$ decomposition components under partial discharge. Appl Surf Sci 315:196–202
21. G. Guoli, Z. Peihong, D. GuangYu, D. Zhenhua (1995) The influence of $SF_6$ and $SF_6/N_2$ dissociating products on the electrical performance of several insulating varnishes, in: Electrical Insulating Materials, 1995. International Symposium on, IEEE. http://ieeexplore.ieee.org/xpls/abs_all.jsp?arnumber=496617. pp. 495–497
22. Zhang X, Yu L, Gui Y, Hu W (2016) First-principles study of $SF_6$ decomposed gas adsorbed on Au-decorated graphene. Appl Surf Sci 367:259–269
23. Zhang X, Gui Y, Dai Z (2015) Adsorption of gases from $SF_6$ decomposition on aluminum-doped SWCNTs: a density functional theory study. Eur Phys J D 69:1–8
24. X. Zhang, L. Yu, X. Wu, W. Hu. Experimental sensing and density functional theory study of $H_2S$ and $SOF_2$ adsorption on Au-modified graphene. Adv Sci. 2 (2015): http://onlinelibrary.wiley.com/doi/10.1002/advs.201500101/full
25. Hoshino T, Nojima K, Hanai M (2004) Real-time PD identification in diagnosis of GIS using symmetric and asymmetric UHF sensors. Power Delivery IEEE Trans 19:1072–1077
26. R. Hu, X. Cui, W. Zhang, P. Chen, L. Qi, J. Li, W. Chen, Z. Li, M. Dai (2012) Transient enclosure voltage (TEV) measurement system of UHV GIS and TEV statistical characterization, in: Electromagnetic Compatibility (EMC EUROPE), 2012 International Symposium on, IEEE. http://ieeexplore.ieee.org/xpls/abs_all.jsp?arnumber=6396743.pp. 1–6
27. Kweon D-J, Chin S-B, Kwak H-R, Kim J-C, Song K-B (2005) The analysis of ultrasonic signals by partial discharge and noise from the transformer. Power Delivery IEEE Trans 20:1976–1983
28. Mangeret R, Farenc J, Ai B, Destruel P, Puretolas D, Casanovas J (1991) Optical detection of partial discharges using fluorescent fiber. Electrical Insulation IEEE Trans 26:783–789
29. Bae C, Yoo H, Kim S, Lee K, Kim J, Sung MM, Shin H (2008) Template-directed synthesis of oxide nanotubes: fabrication, characterization, and applications†. Chem Mater 20:756–767
30. Chang WT, Hsueh YC, Huang SH, Liu KI, Kei CC, Perng TP (2013) Fabrication of Ag-loaded multi-walled $TiO_2$ nanotube arrays and their photocatalytic activity. J Mater Chem A 1:1987–1991
31. Khameneh Asl S, Alavi B, Ahmadi S (2012) The effect of highly ordered titania nanotube structures on hydrogen gas detection. Surf Interface Anal 44:1051–1053
32. Peng T, Yang H, Chang G, Dai K, Hirao K (2004) Synthesis of bamboo-shaped $TiO_2$ nanotubes in nanochannels of porous aluminum oxide membrane. Chem Lett 33:336–337
33. Poudel B, Wang W, Dames C, Huang J, Kunwar S, Wang D, Banerjee D, Chen G, Ren Z (2005) Formation of crystallized titania nanotubes and their transformation into nanowires. Nanotechnology 16:1935
34. Weng L-Q, Song S-H, Hodgson S, Baker A, Yu J (2006) Synthesis and characterisation of nanotubular titanates and titania. J Eur Ceramic Soc 26:1405–1409
35. Li S, Zhang G, Guo D, Yu L, Zhang W (2009) Anodization fabrication of highly ordered $TiO_2$ nanotubes. J Phys Chem C 113:12759–12765
36. Gong D, Grimes CA, Varghese OK, Hu W, Singh R, Chen Z, Dickey EC (2001) Titanium oxide nanotube arrays prepared by anodic oxidation. J Mater Res 16:3331–3334
37. Mor GK, Varghese OK, Paulose M, Shankar K, Grimes CA (2006) A review on highly ordered, vertically oriented $TiO_2$ nanotube arrays: fabrication, material properties, and solar energy applications. Solar Energy Mater Solar Cells 90:2011–2075
38. Xiao FX, Hung SF, Miao J, Wang HY, Yang H, Liu B (2015) Metal-cluster-decorated $TiO_2$ nanotube arrays: a composite heterostructure toward versatile photocatalytic and photoelectrochemical applications. Small 11:554–567
39. Jeun JH, Park KY, Kim DH, Kim WS, Kim HC, Lee BS, Kim H, Yu WR, Kang K, Hong SH (2013) SnO2@ $TiO_2$ double-shell nanotubes for a lithium ion battery anode with excellent high rate cyclability. Nanoscale 5:8480–8483
40. Zhang X, Zhang J, Jia Y, Xiao P, Tang J (2012) $TiO_2$ nanotube array sensor for detecting the SF6 decomposition product SO2. Sensors 12:3302–3313
41. Zhang X, Chen Q, Hu W, Zhang J (2013) A DFT study of $SF_6$ decomposed gas adsorption on an anatase (101) surface. Appl Surf Sci 286:47–53
42. Zhang X, Chen Q, Tang J, Hu W, Zhang J (2014) Adsorption of $SF_6$ decomposed gas on anatase (101) and (001) surfaces with oxygen defect: a density functional theory study. Sci Rep 4:4762
43. Zhang X, Tie J, Chen Q, Xiao P, Zhou M (2015) Pt-doped $TiO_2$-based sensors for detecting $SF_6$ decomposition components. Dielectrics Electrical Insulation IEEE Trans 22:1559–1566